Experimental dynamic characterization of a new composite glubam-steel truss structure

Giuseppe Quaranta[a], Cristoforo Demartino[b,*], Yan Xiao[c]

[a] *Department of Structural and Geotechnical Engineering, Sapienza University of Rome Via Eudossiana 18, 00184 Rome, Italy*

[b] *College of Civil Engineering, Nanjing Tech University, 30 South Puzhu Road, 211816 Nanjing, P.R. China*

[c] *Zhejiang University - University of Illinois at Urbana Champaign Institute, 718 East Haizhou Road, 314400 Zhejiang, P.R. China*

Abstract

The main characteristics of an original bamboo-steel composite truss structure are presented in this work. Specifically, the considered system is a spatial truss structure whose upper chord and diagonal bars are made by glubam elements whereas its lower chord is made by steel members with a hollow cross-section. This novel structural system has been conceived to build roofs and low/mid-span bridges (for example, footbridges), in such a way to ensure easy and rapid construction, efficient use of the constituent materials, low manufacturing costs and good environmental sustainability. A prototype spatial truss beam for laboratory tests is initially described by providing details about geometry, connections and materials properties. The results obtained from dynamic experimental tests are then discussed. In particular, the dynamic response under ambient vibrations and the free-decay response of this truss structure have been recorded and analyzed in order to estimate its modal properties. Design values of the viscous damping ratio for glubam truss structures with steel bolted connections are finally recommended. The numerical assessment of the human-induced vibration serviceability conditions for footbridges built by means of this structural system is finally performed.

Keywords: Damping; Dynamic identification; Glubam; Spatial truss structure; Vibration performance.

*Corresponding author.

Preprint submitted to Journal of Building Engineering

1. Introduction

Nowadays, there is an increasing interest in the use of bamboo-based products for civil constructions. Its most appealing features are attributable to the fact that bamboo is a highly renewable construction material with low embodied energy and high strength-to-weight ratio. Bamboo is used in rural housing and scaffolding mainly in South Asia and South America for many years. Moreover, the use of small diameter culm and/or split bamboo has been proposed as an alternative to reinforcing steel in reinforced concrete [4]. The structural use of this material in modern light-frame buildings is also under investigation, see for instance Wang et al. [38]. The possibility of using bamboo as building material for modern structures in Western countries has been addressed in van der Lugt et al. [23]. Herein, the authors applied the Life Cycle Analysis to the largest bamboo-made structural projects in Western Europe at that time (namely, a bamboo tower, a pedestrian bridge, two pavilions, and an open-air theater). Through a comparative analysis based on environmental and financial aspects, they demonstrated that bamboo can compete with building materials more commonly used in these countries. Mahdavi et al. [24] considered the laminated bamboo lumber from different perspectives and concluded that it can be economically, environmentally and, perhaps, structurally valid choice. Further useful insights about the potential of bamboo as sustainable building material have been presented by Escamilla and Habert [16].

Several efforts have been spent to gain a reliable appraisal of the mechanical properties of bamboo in view of its use as a structural material. For instance, Dixon et al. [14] investigated the flexural properties of some species of bamboo – namely, Moso, Guadua and Tre Gai – by means of three-point bending tests. As regards the elastic moduli of these species, it was found that they largely depend on the density. Specifically, the elastic modulus of Moso exhibited the least scatter with respect to density. On the other hand, the elastic modulus of the Guadua was found higher than that of Moso and Tre Gai for a given density. The effects of two processing methods (i.e., bleaching and caramelization) on the mechanical properties of engineered bamboo were investigated by Sharma et al. [33]. The flexural fatigue behavior of bamboo has been studied by Song et al. [35], who also proposed a Weibull function to evaluate the probability of failure of bamboo strips subjected to flexural loading. Studies by Amada and Lakes [3] explored at the material level the viscoelastic properties of bamboo in torsion and bending using the resonance half-width method at a temperature of 22 °C. For dry bamboo, values of the loss factor of about 0.01 in bending and from 0.02 to 0.03 in torsion have been found whereas they vary from 0.012 to 0.015 in bending and from 0.03 to 0.04 in torsion for wet bamboo. These results are comparable with those for woods: for instance, spruce and beech exhibit loss factor of about 0.02 at room temperature (about 27 °C). These findings were recently confirmed by Habibi et al. [18].

Besides the researches on the mechanical properties of bamboo, several studies have been conducted in order to develop engineered bamboo products and more efficient production processes. A new glue-laminated bamboo material (trademarked as GluBam©) was introduced by Xiao et al. [41, 42] whereas bamboo scrimber and laminated bamboo sheets have been reviewed in Sharma et al. [32]. The need of proper structural details (e.g., joints and connections) has also originated a significant deal of studies [e.g., 5, 27, 44, 22, 15, 31].

Conversely, there are few studies on large-scale structural systems made of bamboo. In this field, Albermani et al. [2] presented a double layer grid that consists of bamboo culms assembled by means of special PVC joints and also built a prototype module of this spatial structure, which was tested under static loads. A 10 m long roadway bridge was designed by Xiao et al. [41] employing glubam girders. The bridge was tested under static loads due to a truck with a total weight of 86 kN. Xiao et al. [43] tested a roof plane truss system made of glubam under static loads. Experimental tests were carried out for two configurations with spans equal to 5 m and 6 m. Another prototype spatial truss structure has been developed in Villegas et al. [37] using bamboo slats in place of bamboo culms and special joints designed for this system. This prototype structure was tested under static loads. Paraskeva et al. [26] designed a bamboo footbridge for rural areas with a span of 8 m. The footbridge was realized by using bamboo culms whereas the connections were realized with bolts and specially designed steel plates. It was tested under static loads reaching a maximum capacity of about 2.50 kN/m^2. As regards the case of dynamic loading conditions, the feasibility of bamboo culms for lattice towers intended for small wind turbines has been analyzed in Adhikari et al. [1] through numerical simulations only. Recently, Wu and Xiao [40] introduced a new type of hybrid truss system composed by glubam (for web and upper chord members) and steel tubes (for lower chord members). They investigated the static performances of this structure finding a good load carrying capacity and concluding that they are suitable for applications in roofs and canopies.

Notably, none of the existing studies has addressed the experimental dynamic assessment of large-scale bamboo structures. This inevitably precludes a proper appraisal of structural systems under dynamic loads, e.g., lattice towers under wind loads, heavy roofs under seismic accelerations as well as footbridges under human-induced vibrations.

In order to fill the gap in the current literature devoted to the characterization of modern bamboo constructions, this study presents some experimental results intended to provide practical guidelines for the analysis and design of glubam structures under dynamic loads. Specifically, an original bamboo-steel composite structure is considered. It is a spatial truss whose upper chord and diagonal bars are made by glubam elements whereas the lower chord is made by steel members with a hollow cross-section. This structure is the same reported in Wu and Xiao [40] that can be considered the companion paper of the present study. While Wu and Xiao [40] focus on design and experimental testing under static loads, the present study deals with the dynamic behavior of such structural system. Initially, the prototype spatial truss beam realized for laboratory dynamic tests is described by providing details about geometry, connections and materials properties (Section 2). The results obtained from dynamic experimental tests are then discussed (Section 3). The main original and valuable contribution of the present work is concerned with the estimation of the viscous damping ratio, for which general recommendations are provided to support the analysis and design of glubam truss structures (Section 4). The assessment of the human-induced vibration serviceability conditions for footbridge use are also investigated (Section 5). In particular, it is addressed the case of application to footbridges of minor importance, which are typically characterized by short/medium span lengths, few non-structural elements and occasional passage of walkers. Finally, the conclusions give a brief summary of the main

Figure 1: Tested composite glubam-steel truss structure.

findings (Section 6).

2. Composite glubam-steel spatial truss structure

2.1. Concept

A composite glubam-steel truss system is considered in the present study. This structure is the same reported in Wu and Xiao [40], in which additional information (including details about the design and data about the materials strength) is provided. This structural system is mainly intended to build roof systems and low/mid-span bridges (especially footbridges). Its upper chord and diagonal bars are made by glubam while steel bars are adopted at the lower chord. In fact, in serviceability conditions, the most relevant limit state for the diagonal bars and the bars of the upper chord is related to the instability under compression forces. By using glubam members with solid cross-sections and high inertia values, the buckling load is increased. On the other hand, the most relevant limit state for the bars of the lower chord is due to the tension force, and thus hollow thin-walled steel elements are deemed appropriate. The modular geometry of the structure facilitates its industrial production and requires minimum work at the construction site for the final assembly thanks

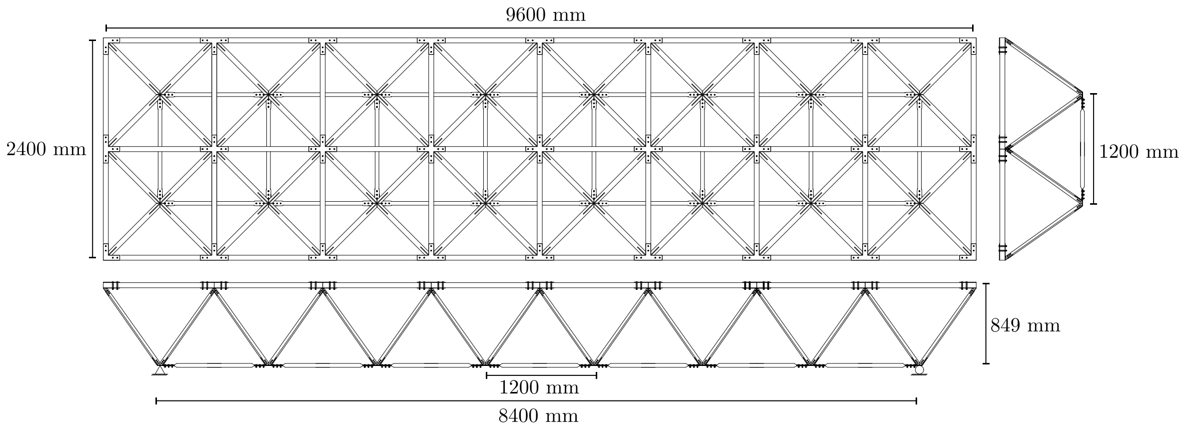

Figure 2: Spatial geometry of the composite glubam-steel truss structure.

to its connections, thereby allowing the reduction of the overall cost. Apart from the use of bamboo, another important environmental benefit is due to the use of reversible connections, which allow for separating each bar of the truss structure from the others at the end of its life-cycle without damages, so as they can be eventually reused for another construction.

2.2. Prototype composite truss structure

The tested composite bamboo-steel structure is shown in Figure 1. The spatial geometry of this truss beam consists of 2×8 identical square pyramids (the vertex of which is on the bottom chord), see Figure 2. It can be noted that non-structural elements are not considered in this prototype structural system. The base of each module is 1200 mm × 1200 mm whereas the height is 849 mm. Therefore, the in-plane dimension of this spatial structure is 2400 mm × 9600 mm. The bars made of glubam have a square cross-section whose size is 56 mm × 56 mm. These bars are built by gluing 9 smaller square elements (each one composed of 3 or 4 thin bamboo strips) through a 3×3 arrangement. The steel bars of the lower chord have a hollow circular cross-section whose external diameter and wall thickness are equal to 42 mm and 4 mm, respectively. The total weight of the structure is about 460 kg and the average weight per unit of length and unit of area are 55 kg/m and 22 kg/m^2, respectively. The first two nodes on one side of the lower chord are constrained by means of two hinges. On the other side, there are two rollers. The length of this truss beam can be considered representative of the typical span for small roofs or footbridges. Accordingly, it can be

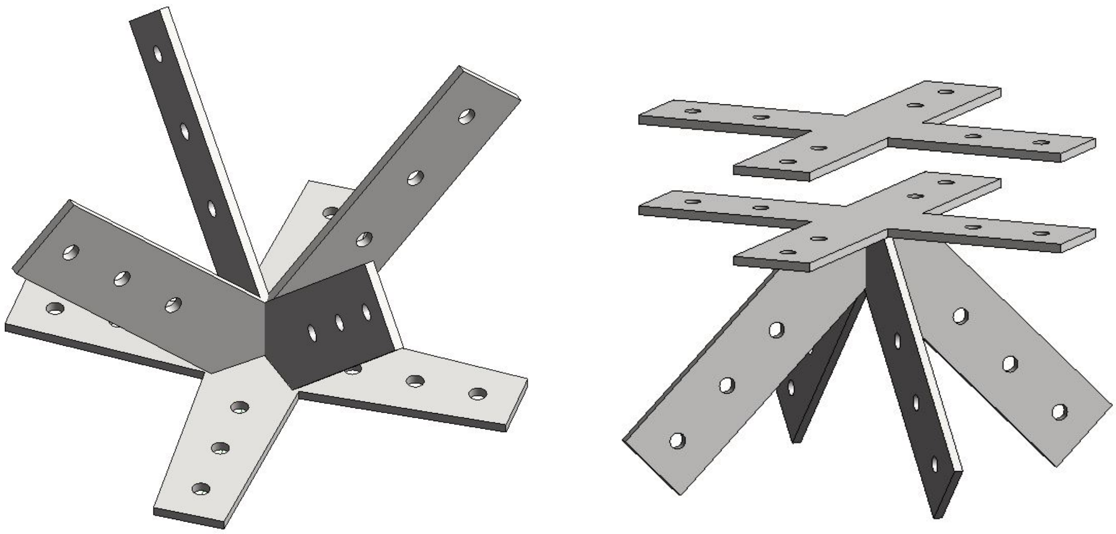

Figure 3: Steel connections of the truss structure: bottom nodes (left) and upper nodes (right).

considered as a full-scale prototype.

All the members of this space truss system are assembled by means of steel connections (Figure 3). Two types of connections have been designed for the upper and lower chords, which are adapted depending on the specific number of ways at the considered node.

In all the connections, 4.8-grade bolts with a diameter of 10 mm have been used. A total of three bolts have been adopted in the ways connecting the elements of the lower chord and the diagonal bars while two bolts have been used for the elements of the upper chord.

Finally, given the innovative nature of the truss structure, it is opportune to provide the unitary cost of the members adopted and the cost per unit of length of the materials. The costs per unit of volume are estimated using reference values based on small quantity production, rather than mass production, which are reasonable for China at the time when this research work has been carried out. The volumetric cost for glubam is about 8000-10000 yuan (about $1200-1500) per cubic meter while that of steel tube is about 35000-40000 yuan (about $5000-6000) per cubic meter.

The spatial truss system (see Figure 1) is made of 106 glubam bars corresponding to a volume of about $0.4\,\mathrm{m}^3$ and of 22 steel bars corresponding to a volume of about $0.07\,\mathrm{m}^3$. It can be seen that the amount of steel in terms of volume is much less compared with the glubam (see Figure 1). Neglecting the joints, the indicative cost for a single member is:

$$\begin{aligned} 1.2\,\text{m} \times (0.056\,\text{m})^2 \times 9000\,\text{yuan/m}^3 &\cong 34\,\text{yuan} \quad \text{for glubam} \\ 1.2\,\text{m} \times \pi \left[\left(\frac{0.042}{2}\text{m} \right)^2 - \left(\frac{0.038}{2}\text{m} \right)^2 \right] \times 38000\,\text{yuan/m}^3 &\cong 11\,\text{yuan} \quad \text{for steel} \end{aligned} \tag{1}$$

The total cost of the material can be calculated as $106 \times 34\,\text{yuan} + 22 \times 11\,\text{yuan} \cong 3850\,\text{yuan}$. The final cost per unit of length of the material employed in the structure is about $3850\,\text{yuan}/9.6\,\text{m} \cong 400\,\text{yuan}$. It should be highlighted that these costs only refer to the material, whereas manufacturing and installation costs are neglected.

As a final note, it might be worth to mention that the cost for glubam is based on small volume trial manufacturing order and the cost may be reduced in possible future mass production.

2.3. Materials properties

The density of glubam and steel adopted within this structural system is equal to 737 kg/m^3 and 7850 kg/m^3, respectively. Standard tension tests for the materials were conducted and the strain-stress curves of the materials are illustrated in Figure 4. The average tensile strength of steel is 513 MPa and the average yield strength is 420 MPa. The average compressive strength of the glubam is 67.72 MPa and its elastic modulus is 10.1 GPa. The moisture content of the glubam specimen measured before the tests ranged from 6% to 7%. The results show that the glubam used in this study is comparable in terms of compressive strength with common laminated bamboo described in the literature [e.g., 21, 12].

3. Dynamic identification

3.1. Equipments and testing protocols

The dynamic response of the structure has been recorded by means of a network of uniaxial piezoelectric accelerometers Lance-LC0115 (Lance Technologies Inc., Qinhuangdao, Hebei, P.R. China) whose properties are the following: sensitivity 5 V/g, frequency range

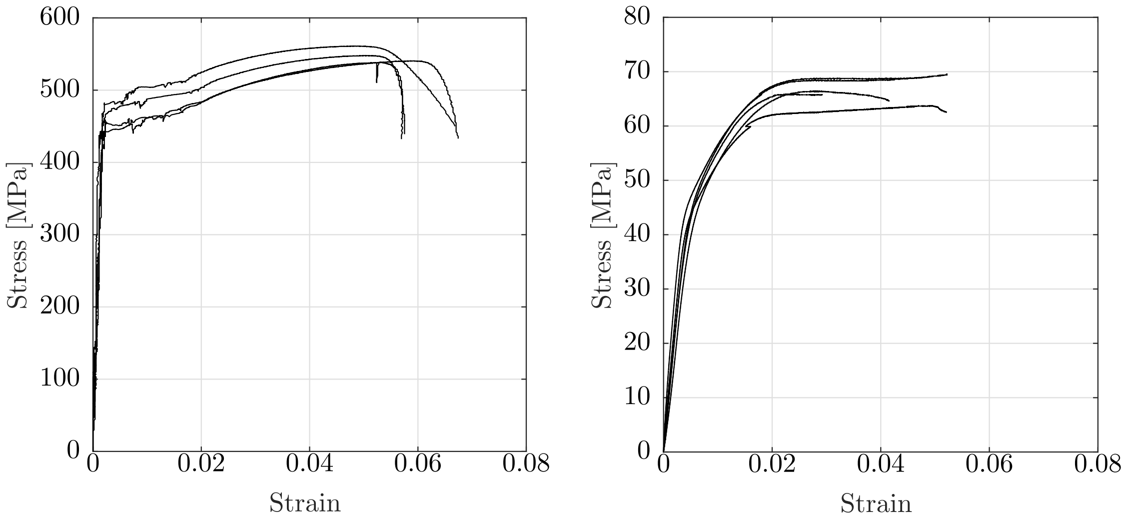

Figure 4: Strain-stress curves of the materials: steel (left) and glubam (right).

0.1 Hz – 1500Hz, resolution 0.000004 g, full-scale range ± 1 g. The data acquisition system was the National Instruments NI PXI-1042Q equipped with the software NI Signal Express 2014. The adopted sampling rate was 1 kHz. The acceleration response of the truss structure has been recorded under two dynamic loading conditions.

The first dynamic loading scenario consists of ambient vibrations basically attributable to the movements of small vehicles inside the laboratory and to the passage of heavy vehicles on the roads near to it. In this case, the length of the time recordings was equal to 20 min. All the free joints were equipped with an accelerometer with the exception of the three nodes at the beginning and the end of the upper chord. The vertical component and the horizontal component orthogonal to the longitudinal axis of the truss structure have been recorded by means of several layouts in which some sensors were moved while six accelerometers were left in their original positions to keep track of the phase.

The second dynamic loading scenario is the free-decay response of the truss structure, which has been induced by removing suddenly a mass of 35 kg originally suspended at the midspan of the bottom chord. The free-decay response has been recorded over a time-window whose length was equal to 15 s. In this case, a single layout consisting of eight measurement points on the upper chord was employed to record the vertical response. Specifically, three accelerometers were regularly spaced on both sides of the upper chord whereas two other

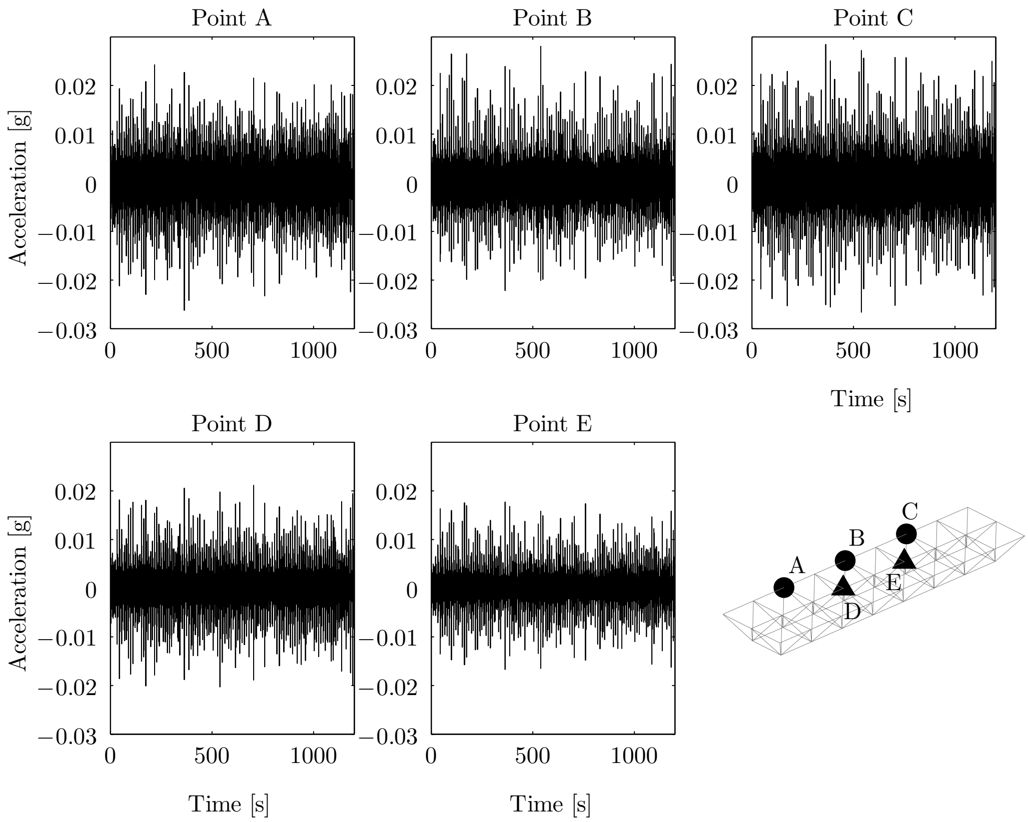

Figure 5: Some samples of the acceleration response recorded under ambient vibrations (circular markers: vertical direction, triangular markers: horizontal direction perpendicular to the longitudinal axis).

accelerometers were installed along the longitudinal axis.

3.2. Operational modal analysis using ambient vibrations

The response of the truss structure under ambient vibrations (see some samples in Figure 5) has been elaborated in frequency- and time-domain in order to identify its modal parameters. Enhanced Frequency Domain Decomposition (EFDD) and Stochastic Subspace Identification (SSI) have been adopted for output-only modal parameter estimation. Theoretical details about these techniques can be found elsewhere [e.g., 25, 8, 7, 36].

In the first step, the vertical accelerations only have been considered in the dynamic identification process while the horizontal components have been neglected. A total of five modes of vibration have been identified. The corresponding natural frequencies and damping ratios are listed in Table 1 whereas the operational modal shapes are shown from Figure 6

Table 1: Natural frequencies and damping ratios identified from the vertical response recorded under ambient vibrations by means of EFDD and SSI (in the latter case, the standard deviation value is reported within the brackets).

Mode	EFDD		SSI	
	Frequency [Hz]	Damping [%]	Frequency [Hz]	Damping [%]
1	21.8	1.532	21.74 (0.2099)	1.686 (0.4141)
2	33.58	0.8126	33.54 (0.0971)	0.7068 (0.315)
3	42.18	0.7421	41.56 (0.2097)	0.8128 (0.4714)
4	56.66	1.415	56.5 (0.2783)	1.4 (0.2632)
5	73.25	0.6987	N/A	N/A

to Figure 10 (herein, the nodes that were not equipped with a sensor are not shown).

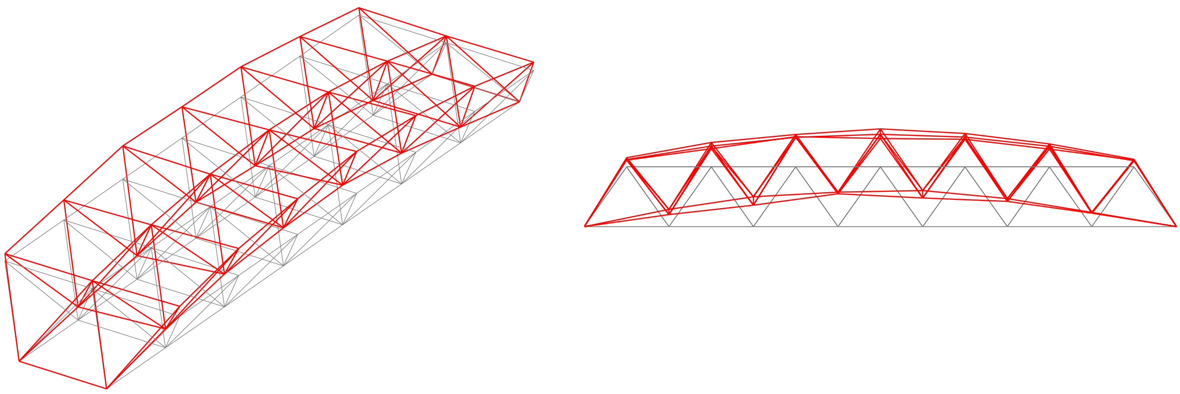

Figure 6: First mode of vibration identified from the vertical response recorded under ambient vibrations by means of EFDD (natural frequency 21.8 Hz, damping ratio 1.532%).

Overall, there is an excellent agreement between the results obtained from EFDD and those carried out by means of the SSI technique (see Table 1). The fundamental modal shape is a bending-type mode of vibration (see Figure 6). The second and third mode of vibration are the first and the second torsional modal shapes, respectively (see Figure 7 and Figure 8). Finally, the fourth and fifth modal shapes are the second and the third bending-type mode of vibration. Deviations in the operational modal shapes from the ideal ones are basically attributable to uncertainties in boundary conditions and structural details (such as the preload conditions of the bolted joints, which were not monitored during the assembly of the structure). The deviation is evidenced by the non-perfect symmetry in symmetric

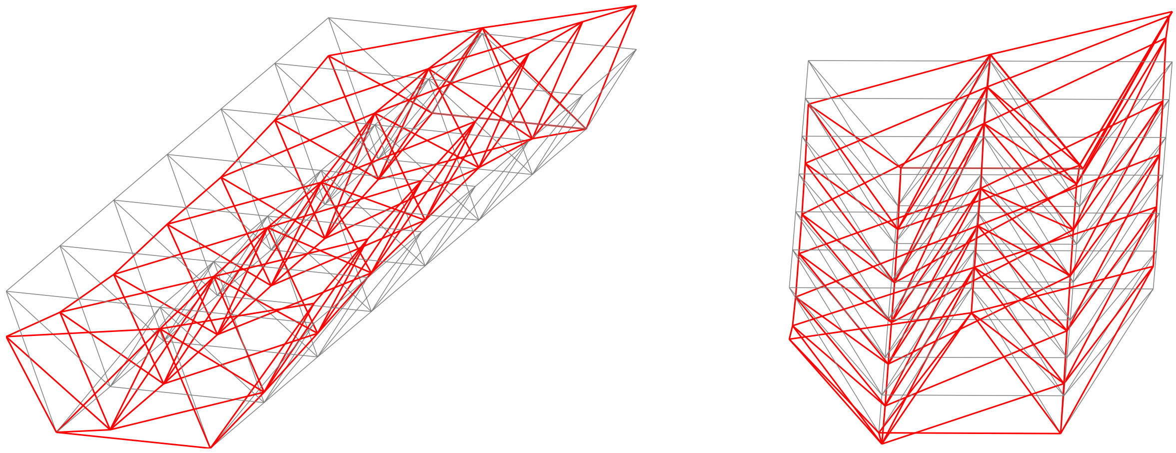

Figure 7: Second mode of vibration identified from the vertical response recorded under ambient vibrations by means of EFDD (natural frequency 33.58 Hz, damping ratio 0.8126%).

Table 2: Natural frequencies and damping ratios identified from ambient vibrations by means of EFDD using the vertical response only or, both, horizontal and vertical responses.

Mode	Vertical response		Vertical and horizontal response	
	Frequency [Hz]	Damping [%]	Frequency [Hz]	Damping [%]
1	21.8	1.532	21.11	1.538
2	33.58	0.8126	33.97	0.7332
3	42.18	0.7421	41.92	0.8441
4	56.66	1.415	56.49	1.739
5	73.25	0.6987	73.37	0.572

mode shapes and non-perfect asymmetry in asymmetric mode shapes.

Including the horizontal response orthogonal to the longitudinal axis does not affect the estimates of natural frequencies and damping ratio, as it can be inferred from Table 2. The identified modal shapes do not change when considering the horizontal response, with the only exception of the second mode of vibration. In this case, the identification based on both components of the dynamic response has revealed that the first torsional modal shape occurs with a significant lateral swinging (see Figure 11). This highlights the existence of a strong coupling between the first torsional mode and the first bending-type mode of the truss structure in the horizontal plane.

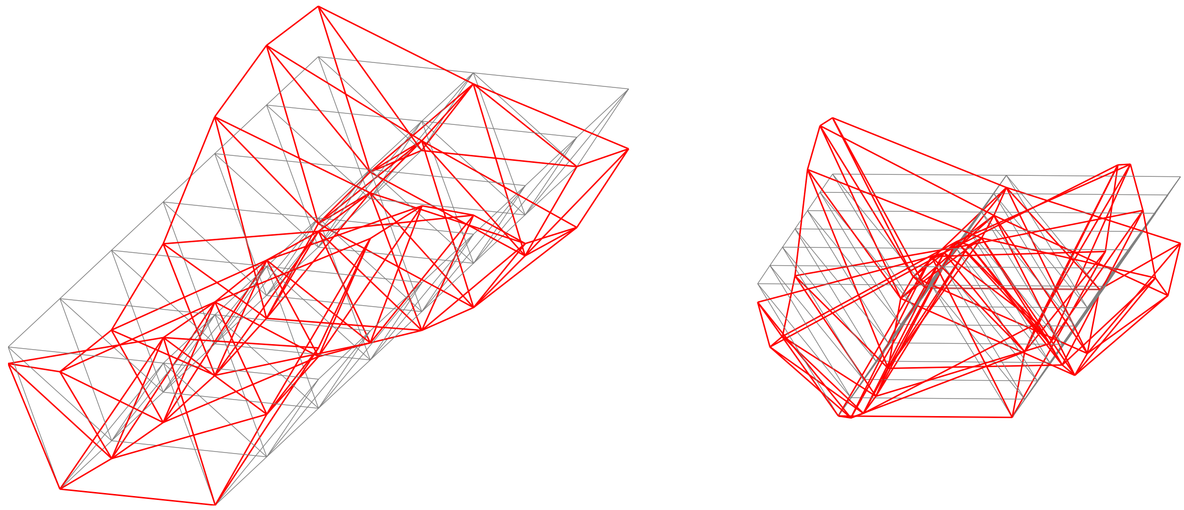

Figure 8: Third mode of vibration identified from the vertical response recorded under ambient vibrations by means of EFDD (natural frequency 42.18 Hz, damping ratio 0.7421%).

3.3. Identification based on the free-decay response

The recorded free-decay vertical response of the truss structure has been analyzed using standard spectral analysis to estimate the natural frequencies whereas the logarithmic decrement technique was employed in order to calculate the damping ratios. A band-pass filtering technique based on the Butterworth filter was used to isolate the mode of vibration detected in the spectral analysis whereas the corresponding damping ratio was evaluated from the logarithm of the instantaneous amplitude obtained through the Hilbert transform. The interested reader can find the theoretical basis of the logarithmic decrement technique elsewhere [e.g., 34].

The analysis of the free-decay response has allowed the identification of natural frequencies and damping ratios for the first and second modes of vibration. The damping identification for the first torsional mode of vibration from a lateral measurement point at the midspan of the truss structure is shown in Figure 12.

Overall, the elaboration of the available recordings has provided the results reported in Table 3 (as regards the outcomes related to the free-decay response, the average values of the results obtained from all the analyzed time-histories are listed). It is possible to observe that they are in very good agreement with the outputs of the operational modal analysis.

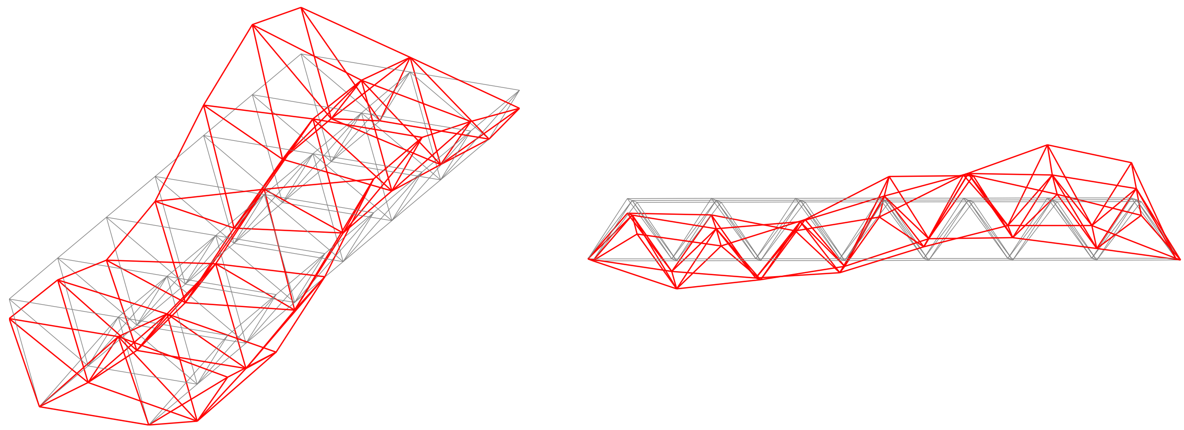

Figure 9: Fourth mode of vibration identified from the vertical response recorded under ambient vibrations by means of EFDD (natural frequency 56.66 Hz, damping ratio 1.415%).

Table 3: Comparison of natural frequencies and damping ratios of the first two modes of vibration identified from the vertical response recorded under ambient vibrations (by means of EFDD) and using the free-decay response.

Mode	Ambient vibrations		Free-decay response	
	Frequency [Hz]	Damping [%]	Frequency [Hz]	Damping [%]
1	21.8	1.532	20.48	1.454
2	33.58	0.8126	33.57	0.744

4. Recommended viscous damping ratio

Since the damping ratio plays a fundamental role in the dynamic behavior of structures such as roof systems and footbridges, it is very important to provide reliable recommendations in this regard to support the analysis and design stages. In this perspective, damping ratios (in percentage) suggested by some standards and guidelines for footbridges made of steel and timber (the two materials relevant for the present study) are summarized in Table 4. This latter is adapted from Demartino et al. [13]. The values refer to the fundamental mode of vibration. It can be observed from Table 4 that lower damping values apply to steel bridges whereas larger values occur in timber bridges. In general, it is known that damping may be divided into three classes [39], namely: internal friction throughout the material making up the structure (material damping), energy dissipation associated with junctions

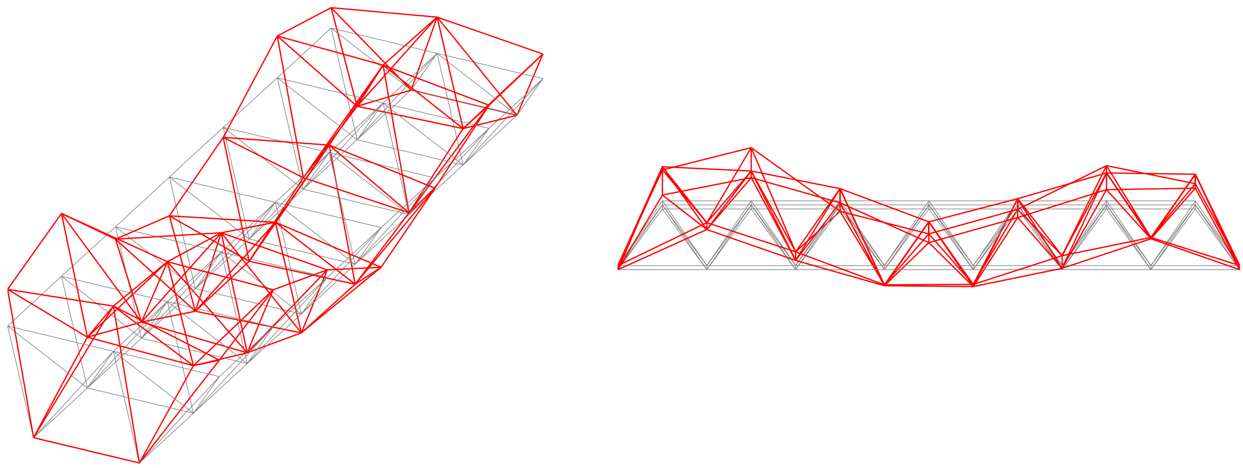

Figure 10: Fifth mode of vibration identified from the vertical response recorded under ambient vibrations by means of EFDD (natural frequency 73.25 Hz, damping ratio 0.6987%).

or interfaces between parts of the structure (structural damping), and energy dissipation associated with a fluid in contact with the structure (fluid damping). The additional effect of the structural damping is considered by Eurocodes. In particular, for steel structures, it is suggested 0.2% for welded connections while 0.4% for bolted connections (which are more dissipative). On the other hand, for timber structures, it is suggested 1% for welded connections (i.e., welded steel socket or brackets) while 1.5% for bolted connections.

The current study found that the damping ratio at the fundamental frequency of the considered composite glubam-steel truss structure is around 1.5%. This result is compatible with that of timber footbridges (Table 4). In particular, the measured damping ratio for the fundamental frequency almost coincides with that suggested for timber structures by Eurocodes if mechanical joints are present (Table 4). Moreover, this value is compatible with Hivoss [19] and FIB [17]. Larger values are suggested by Sétra [30], with a minimum value of 1.5% comparable with the measured one and a maximum value twice the minimum one (i.e., 3.0%). According to the experimental data as well as to the values proposed in Standards and Code of Practice, a viscous damping ratio equal to 1.5% can be recommended for the fundamental (bending-type) mode of glubam truss structures with bolted connections.

It is important to remark that damping ratios identified in this study refer to a system

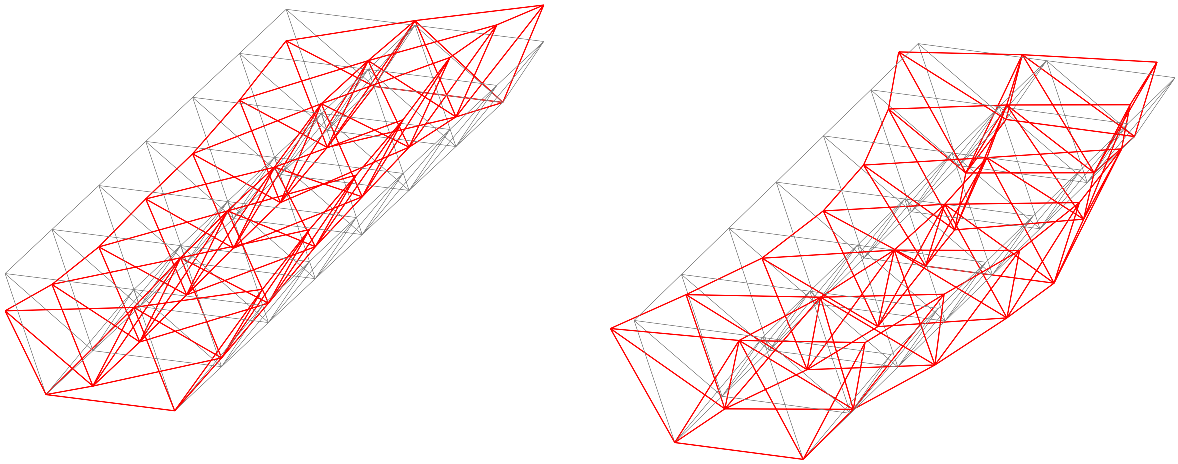

Figure 11: Effects of the horizontal motion on the identification of the second mode of vibration from ambient vibrations by means of EFDD: identification using the vertical response only (left) and identification using both vertical and horizontal response (right).

without non-structural elements, such as roof covering (for roof systems) or deck surface (for footbridges). However, it has been recognized that non-structural elements can have a significant influence on the dissipative properties, i.e., non-structural elements typically increase the damping ratios. Accordingly, in real operative conditions (i.e., with non-structural elements in place), the damping ratios are likely to be higher with respect to those measured in this study which, as a consequence, can be considered as conservative estimates.

5. Assessment of the serviceability conditions for glubam-steel footbridges

The proposed new composite glubam-steel truss structure can be used for footbridges of minor importance, which are typically characterized by short/medium span lengths, few non-structural elements and occasional passage of walkers.

To assess the performance for footbridge use of the proposed structure, the serviceability conditions to a single walker crossing are studied by using the deterministic framework proposed by Demartino et al. [13]. The latter procedure was chosen because suitable for footbridges of minor importance characterized by the occasional passage of walkers that can be modeled as a single walker crossing condition. In particular, to evaluate the human-induced vibrations [29], it is necessary to define the characteristics of the walker (i.e., modal

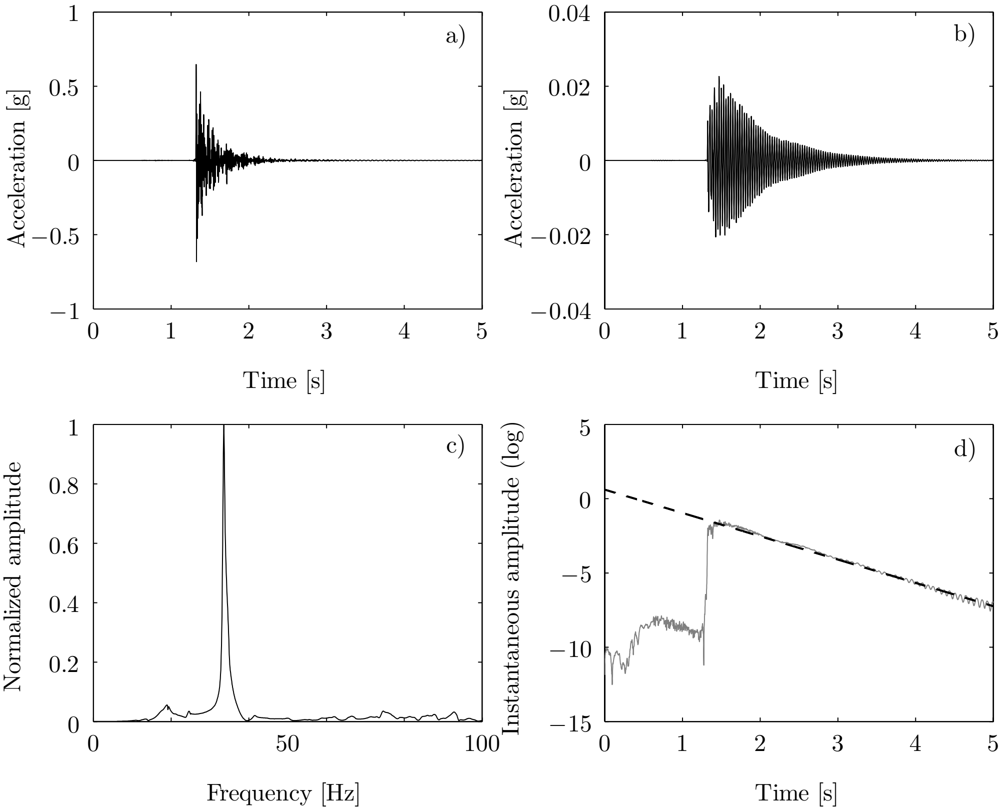

Figure 12: Damping identification for the second mode from the free-decay vertical response recorded at point B (see Figure 5): a) acceleration time-history, b) acceleration time-history after band-pass filtering with respect to the second mode, c) normalized frequency spectrum of the recorded acceleration response after band-pass filtering with respect to the second mode, d) log-scale instantaneous amplitude and best-fit line for damping estimation.

Table 4: Damping ratios (in percentage) for footbridges realized using steel and timber, as given by different standards and guidelines.

Type	Sétra [30]		Hivoss[1]		ISO [20]	Eurocodes[2]	FIB [17]	
	Min	Mean	Min	Mean	Mean	Mean	Min	Mean
Steel	0.2	0.4	0.2	0.4	0.5	0.2/0.4[3]	0.5	1.0
Timber	1.5	3.0	1.0	1.5	-	1/1.5[4]	0.8	1.4

[1] See [19].
[2] EC1 [9], EC3 [10], EC5 [11].
[3] 0.2% if welded connections are present, 0.4% for bolted connections.
[4] 1% if no mechanical joints are present, 1.5% otherwise.

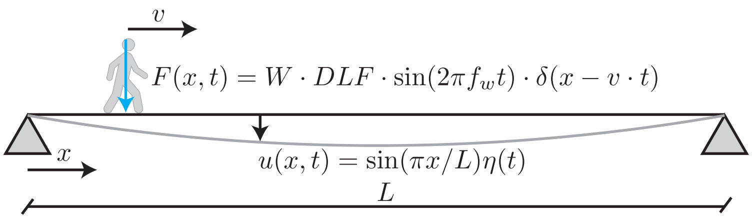

Figure 13: Dynamic model of the simply supported beam in the vertical direction: first mode and walker-induced loads. (x: beam axis with zero coordinate in one support; t: time; v: constant speed of the walker; W: body weight; DLF: dynamic load factor; f_w: walking frequency; δ: Dirac function; L: length of the beam; $u(x,t)$: displacement of the beam at the point x and time t; $\eta(t)$: modal displacement at the time t).

force) and the dynamic properties of the footbridge (i.e., mechanical model).

The modal force is calculated using the characteristics of the standard walker described in Demartino et al. [13]. The mechanical model is a simply supported beam loaded by a constant-speed moving harmonic load for which only the first vertical mode is considered (Figure 13). This is in agreement with the modal shape observed (see Section 3.2). The peak of the modal response is expressed in terms of a transient frequency response function, φ, that is the ratio between the modal peak non-stationary response induced by a given walker crossing the bridge and the corresponding stationary response induced by the standard walker. Being $\sin(\pi/2) = 1$, the peak acceleration in the midspan (i.e., for $x = L/2$) and the peak modal acceleration are the same (see Figure 13):

$$\hat{\ddot{u}}(L/2,t) = \hat{\ddot{\eta}}(t) \cdot \sin(\pi/2) = \hat{\ddot{\eta}}(t) \cdot 1 \tag{2}$$

The peak modal acceleration can be expressed in terms of φ as:

$$\hat{\ddot{u}}(L/2,t) = \frac{DLF \cdot W}{2\xi \cdot m} \cdot \varphi \tag{3}$$

where $DLF = 0.35$ is the dynamic load factor that is the harmonic load amplitude normalized by the body weight $W = 744\,\mathrm{N}$, ξ is the damping ratio and m is the modal mass (half of the total mass for a simply supported beam).

Using the assumptions reported above, it can be used the closed-form solution of φ provided in Ricciardelli and Briatico [28]. Generally speaking, φ is a function of: (i) $\alpha =$

f_w/f: the frequency ratio that is the ratio between the walking frequency $f_w = 1.898\,\mathrm{Hz}$ [13], to the fundamental frequency of the footbridge, f; (*ii*) L: the span of the footbridge (see Figure 13); (*iii*) ξ.

φ is reported in Figure 14 (a) in the range of span length from $L = 5 - 25\,\mathrm{m}$ and $\alpha = 0.01 - 1.2$ for a damping ratio of $\xi = 1.5\%$. The damping ratio is assumed as that identified for the first vertical mode of this structure (see Table 3). It is noteworthy that the viscous damping ratio estimates obtained in the present study (see Section 4) are expected to be very close to real conditions for such class of footbridges, because of the negligible influence of the number pedestrians (due to the single walker crossing conditions) and small impact of non-structural elements [e.g., 6].

The asterisk in Figure 14 indicates the characteristics of the structure of this study, i.e., $L = 8.4\,\mathrm{m}$ and $\alpha = 1.898\,\mathrm{Hz}/21.8\,\mathrm{Hz}$=0.0871. It can be observed that the expected acceleration induced by the crossing of a pedestrian are quite low for this structure (low values of φ). The proposed structure is relatively short ($L = 8.4\,\mathrm{m}$, see Figure 1) and capable of withstanding high-loads as demonstrated in Wu and Xiao [40]. Consequently, it is possible to adopt the same modular system for larger spans expecting lower frequencies corresponding to values of α closer to the unity (i.e., near to the resonance conditions) thus larger accelerations. The frequency of this modular system as a function of the span can be predicted by calculating the stiffness of an equivalent continuous simply supported beam as:

$$f = \frac{1}{2\pi}\sqrt{\frac{a}{m(L)\cdot L^4}} \text{ with } a = \frac{9.87^2 E\cdot I}{2} \tag{4}$$

where $m(L)$ is the modal mass per unit length that can evaluated as half (i.e., valid for simply supported beam) of the mass of the proposed structure and considering the mass proportional with the length (i.e., constant mass):

$$m(L) = \frac{460\,\mathrm{kg}}{2\cdot 8.4\,\mathrm{m}}L = 27.4\,\mathrm{kg/m}\cdot L \tag{5}$$

The assumption of constant mass and stiffness (i.e., constantly distributed) is reasonable

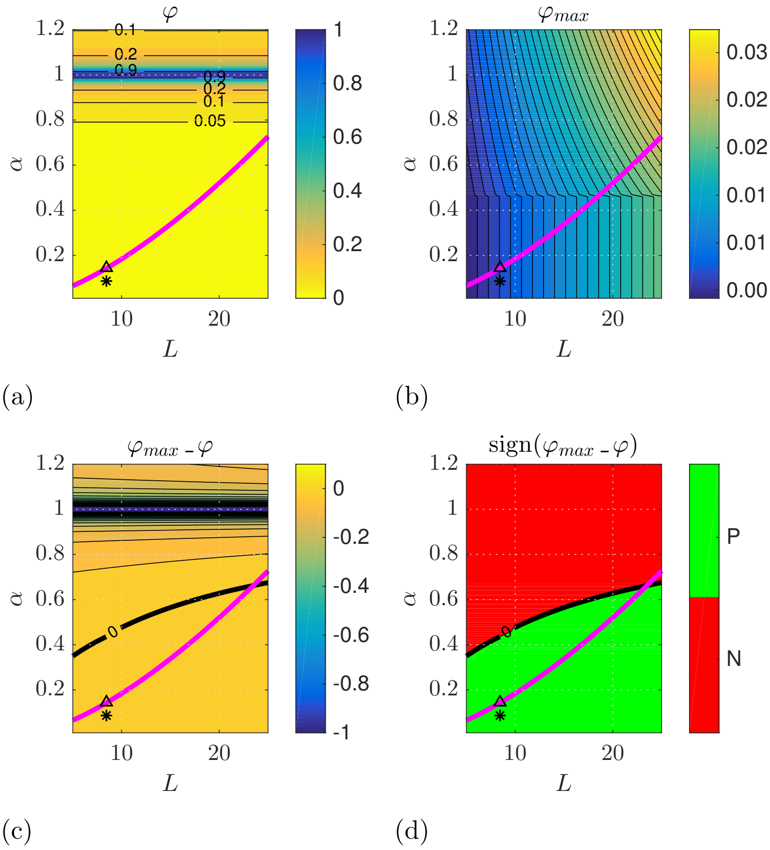

Figure 14: Contour plots in the L-α plane of: φ, (a), maximum tolerable transient frequency response function, φ_{max}, (b), and difference between the demand and capacity, $\varphi_{max} - \varphi$, (c), and its sign (P: positive - verified; N: negative - not verified) (d). The black asterisk indicates the characteristics of the structure of this study. The blue line indicates the frequency variation of an equivalent modular structure as a function of L.

given that the same modular system can be employed for larger spans because of the good static performances [40].

Using Eqs. (4) and (5) and the characteristics of the structure, a can be calculated as:

$$a = f^2 \cdot m(L) \cdot L^3 \cdot (2\pi)^2 = (21.8\text{Hz})^2 \cdot 27.4\,\text{kg/m} \cdot (8.4\text{m})^3 \cdot (2\pi)^2 = 2.56e{+}09\,\text{Hz}^2 \cdot \text{kg} \cdot \text{m}^3 \quad (6)$$

However, the identified frequency is very high (corresponding to low values of the frequency ratio) because the mass is also very low due to the absence of the non-structural elements such as floor and handrails. It is expected that the presence of such elements will slightly decrease the frequency (large values of the frequency ratio) leading to large accelerations. With the aim to provide a more realistic estimation of the serviceability conditions, the mass of the entire footbridge (including the floor and the handrails) is calculated using reasonable values of the weight of non-structural elements. In particular, it is assumed a floor made of common floor gratings for pedestrians areas ($25\,\text{kg/m}^2$) and common steel handrails ($15\,\text{kg/m}^2$). The modal mass per unit length is evaluated as:

$$m(L) = \frac{460\,\text{kg} + (25\,\text{kg/m}^2 \times 8.4\,\text{m} \times 2.4\,\text{m}) + (15\,\text{kg/m} \times 2 \times 8.4\,\text{m})}{2 \cdot 8.4\,\text{m}} L = 72.4\,\text{kg/m} \cdot L \quad (7)$$

The frequency of a modular structure with the same characteristics of the structure investigated in this study but with the addition of the mass of the non-structural elements is predicted combining Eqs. (4), (7) and Eq. (6). The predicted frequency expressed in terms of α is reported in Figure 14 with a thick magenta line. As expected, increasing the span length, the frequency decreases and as a consequence α increases. Moreover, the upward-pointing triangle in Figure 14 indicates the characteristics of the structure of this study but with the addition of the mass of the non-structural elements (as in Eq. 7), i.e., $L = 8.4\,\text{m}$ and $\alpha = 1.898\,\text{Hz}/12.8\,\text{Hz}{=}0.1477$.

A capacity model is needed to assess the serviceability conditions for footbridge use. According to Demartino et al. [13], the maximum tolerable TFRF in the vertical direction is evaluated from the ISO 10137 [20] base curves:

$$\varphi_{max}(\alpha) = \frac{2 \cdot \xi \cdot m}{DLF \cdot W} \begin{cases} 0.21 & \text{if } \alpha \leq 0.47 \\ 0.140 + 0.150 \cdot \alpha & \text{if } \alpha > 0.47 \end{cases} \tag{8}$$

φ_{max} is reported in Figure 14 (b) where the modal mass, m, is taken as in Eq. 7.

The serviceability performance of the structure can be assessed by comparing the deterministic value of the demand, φ, with the deterministic value of the capacity $\varphi_{max}(\alpha)$. Positive values of $\varphi_{max} - \varphi$ indicate verified conditions. $\varphi_{max} - \varphi$ is reported in Figure 14 (c) while its sign in Figure 14 (d).

It can be seen that for low values of L (corresponding to high frequencies and low values of α) the serviceability conditions are always verified (green areas in Figure 14 (d)). In particular, it can be observed that a footbridge realized with this modular structure (magenta line in Figure 14 (d)) is always falling in the verified for $L \leq 23\,\mathrm{m}$ proving its good vibration serviceability performance for footbridge use. It should be highlighted that for $L \geq 23\,\mathrm{m}$ (almost three times the span of the studied structure, see Figure 2) the modular structure should be re-designed to fulfill serviceability checks, for instance by increasing the stiffness.

6. Conclusions

This study investigated the dynamic characteristics of a new composite glubam-steel truss structure in which the elements of upper chords and diagonal bars are made of glued laminated bamboo (glubam) while the bars of the lower chord are made of steel bars with hollow cross-sections. Such a system was conceived to facilitate its industrial production while reducing the overall cost and ensuring high environmental sustainability through efficient use of the constituent materials and structural details suitable to allow the reuse of each element. Laboratory tests were performed on a prototype structural system in order to estimate its dynamic properties.

After a critical review of the experimental evidence, a conservative viscous damping ratio around 1.5% for the fundamental (bending-type) mode is suggested in glubam truss structures with steel bolted connections whereas conservative values between 0.5% and 1.5% (mean value equal to 1%) are recommended for all the modes. Finally, the human-induced vibration serviceability conditions for footbridge use of the proposed structure were assessed. The numerical analyses demonstrated a good dynamic behavior of glubam footbridges of minor importance, thereby supporting the feasibility of this new structural typology in real applications.

Acknowledgments

The research conducted in this paper was supported by National Natural Science Foundation of China (NSFC) through a National General Project (No. 51678296), and the 2016 Jiangsu provincial Double-innovation plan. The authors would like to thank Mr. Yue Wu for having conducted the laboratory tests.

References

References

[1] Adhikari R, Wood D, Sudak L (2015) Low-cost bamboo lattice towers for small wind turbines. Energy for Sustainable Development 28:21 – 28

[2] Albermani F, Goh G, Chan S (2007) Lightweight bamboo double layer grid system. Engineering Structures 29(7):1499 – 1506

[3] Amada S, Lakes RS (1997) Viscoelastic properties of bamboo. Journal of Materials Science 32(10):2693–2697

[4] Archila H, Kaminski S, Trujillo D, Escamilla EZ, Harries KA (2018) Bamboo reinforced concrete: a critical review. Materials and Structures 51(4):102

[5] Aschheim M, Gil-Martón L, Hernández-Montes E (2010) Engineered bamboo i-joists. Journal of Structural Engineering 136(12):1619–1624

[6] Avossa A, Demartino C, Ricciardelli F (2017) Design procedures for footbridges subjected to walking loads: Comparison and remarks. Baltic Journal of Road & Bridge Engineering 12(2)

[7] Brincker R, Ventura C, Andersen P (2001) Damping estimation by frequency domain decomposition. In: Proceedings of 19th International Modal Analysis Conference (IMAC XIX), Orlando, FL (USA)

[8] Brincker R, Zhang L, Andersen P (2001) Modal identification of output-only systems using frequency domain decomposition. Smart Materials and Structures 10:441 – 445

[9] CEN (2003) Eurocode 1: Actions on structures

[10] CEN (2005) Eurocode 3: Design of Steel Structures

[11] CEN (2005) Eurocode 5: Design of timber structures

[12] Correal JF, Echeverry JS, Ramírez F, Yamín LE (2014) Experimental evaluation of physical and mechanical properties of glued laminated guadua angustifolia kunth. Construction and Building Materials 73:105–112

[13] Demartino C, Avossa AM, Ricciardelli F (2018) Deterministic and probabilistic serviceability assessment of footbridge vibrations due to a single walker crossing. Shock and Vibration

[14] Dixon P, Ahvenainen P, Aijazi A, Chen S, Lin S, Augusciak P, Borrega M, Svedström K, Gibson L (2015) Comparison of the structure and flexural properties of Moso, Guadua and Tre Gai bamboo. Construction and Building Materials 90:11 – 17

[15] Echeverry J, Correal J (2015) Cyclic behavior of laminated guadua mat sheathing-to-framing connections. Construction and Building Materials 98:69 – 79

[16] Escamilla E, Habert G (2014) Environmental impacts of bamboo-based construction materials representing global production diversity. Journal of Cleaner Production 69:117 – 127

[17] FIB (2005) Guidelines for the design of footbridges

[18] Habibi MK, Tam LH, Lau D, Yang L (2016) Viscoelastic damping behavior of structural bamboo material and its microstructural origins. Mechanics of Materials 97:184–198

[19] Heinemeyer C, Butz C, Keil A, Schlaich M, Goldack A, Lukić M, Chabrolin B, Lemaire A, Martin P, Cunha A, Caetano E (2009) Design of Lightweight Footbridges for Human Induced Vibrations – Background document in support to the implementation, harmonization and further development of the Eurocodes

[20] ISO (2007) Bases for design of structures – Serviceability of buildigns and walkways against vibration

[21] Li Ht, Zhang Qs, Huang Ds, Deeks AJ (2013) Compressive performance of laminated bamboo. Composites Part B: Engineering 54:319–328

[22] Li Z, Xiao Y, Wang R, Monti G (2015) Studies of nail connectors used in wood frame shear walls with ply-bamboo sheathing panels. Journal of Materials in Civil Engineering 27(7)

[23] van der Lugt P, van den Dobbelsteen A, Janssen J (2006) An environmental, economic and practical assessment of bamboo as a building material for supporting structures. Construction and Building Materials 20(9):648 – 656

[24] Mahdavi M, Clouston P, Arwade S (2011) Development of laminated bamboo lumber: Review of processing, performance, and economical considerations. Journal of Materials in Civil Engineering

23(7):1036–1042

[25] Nisticò N, Gambarelli S, Fascetti A, Quaranta G (2016) Experimental dynamic testing and numerical modeling of historical belfry. International Journal of Architectural Heritage 10(4):476–485

[26] Paraskeva T, Grigoropoulos G, Dimitrakopoulos EG (2017) Design and experimental verification of easily constructible bamboo footbridges for rural areas. Engineering Structures 143:540–548

[27] Ramirez F, Correal J, Yamin L, Atoche J, Piscal C (2012) Dowel-bearing strength behavior of glued laminated *guadua* bamboo. Journal of Materials in Civil Engineering 24(11):1378–1387

[28] Ricciardelli F, Briatico C (2010) Transient response of supported beams to moving forces with sinusoidal time variation. Journal of Engineering Mechanics 137(6):422–430

[29] Ricciardelli F, Demartino C (2016) Design of footbridges against pedestrian-induced vibrations. Journal of Bridge Engineering 21(8):C4015003

[30] Sétra (2006) Technical guide - Footbridges: Assessment of vibrational behaviour of footbridges under pedestrian loading

[31] Shan B, Xiao Y, Zhang W, Liu B (2017) Mechanical behavior of connections for glubam-concrete composite beams. Construction and Building Materials 143:158 – 168

[32] Sharma B, Gatóo A, Bock M, Ramage M (2015) Engineered bamboo for structural applications. Construction and Building Materials 81:66 – 73

[33] Sharma B, Gatóo A, Ramage M (2015) Effect of processing methods on the mechanical properties of engineered bamboo. Construction and Building Materials 83:95 – 101

[34] Shin K, Hammond J (2008) Fundamentals of signal processing for sound and vibration engineers. Wiley

[35] Song J, Utama Surjadi J, Hu D, Lu Y (2017) Fatigue characterization of structural bamboo materials under flexural bending. International Journal of Fatigue 100:126 – 135

[36] Van Overschee P, de Moor BL (1996) Subspace identification for linear systems. Kluwer Academic Publishers

[37] Villegas L, Morán R, García J (2015) A new joint to assemble light structures of bamboo slats. Construction and Building Materials 98:61 – 68

[38] Wang J, Demartino C, Xiao Y, Li Y (2018) Thermal insulation performance of bamboo-and wood-based shear walls in light-frame buildings. Energy and Buildings 168:167–179

[39] Woodhouse J (1998) Linear damping models for structural vibration. Journal of Sound & Vibration 215(3):547–569

[40] Wu Y, Xiao Y (2018) Steel and glubam hybrid space truss. Engineering Structures 171:140–153

[41] Xiao Y, Zhou Q, Shan B (2010) Design and construction of modern bamboo bridges. Journal of Bridge Engineering 15(5):533–541

[42] Xiao Y, Yang R, Shan B (2013) Production, environmental impact and mechanical properties of glubam.

Construction and Building Materials 44:765 – 773
[43] Xiao Y, Chen G, Feng L (2014) Experimental studies on roof trusses made of glubam. Materials & Structures 47(11):1879–1890
[44] Xiao Y, Li Z, Wang R (2014) Lateral loading behaviors of lightweight wood-frame shear walls with ply-bamboo sheathing panels. Journal of Structural Engineering 141(3):B4014004